

# Annealing Induced Saturation in Electron Concentration for V-Doped CdO

Yajie Li <sup>1,2,\*</sup>, Guibin Chen <sup>3</sup>, Kinman Yu <sup>2,4</sup>, Wladyslaw Walukiewicz <sup>2,5</sup> and Weiping Gong <sup>1</sup>

<sup>1</sup> Guangdong Provincial Key Laboratory of Electronic Functional Materials and Devices, Huizhou University, Huizhou 516007, China; gwp@hzu.edu.cn

<sup>2</sup> Materials Sciences Division, Lawrence Berkeley National Laboratory, Berkeley, CA 94720, USA; kinmanyu@cityu.edu.hk (K.Y.); w\_walukiewicz@lbl.gov (W.W.)

<sup>3</sup> Physics Department and Jiangsu Key Laboratory for Chemistry of Low Dimensional Materials, Huaiyin Normal University, Huaian 223001, China; gbchen@hytc.edu.cn

<sup>4</sup> Department of Physics, City University of Hong Kong, Kowloon Tong, Hong Kong 999077, China

<sup>5</sup> Department of Materials Science and Engineering, University of California, Berkeley, CA 94720, USA

\* Correspondence: virjoy\_913@163.com

**Abstract:** As-grown Ar-deposited Cd<sub>1-x</sub>V<sub>x</sub>O and Ar/O<sub>2</sub>-deposited Cd<sub>1-y</sub>V<sub>y</sub>O feature lower and higher electron concentrations than  $4 \times 10^{20} \text{ cm}^{-3}$ , respectively. After isothermal and isochronal annealing under N<sub>2</sub> ambient, we find that the two series exhibit a decrease or increase in electron concentrations until  $\sim 4 \times 10^{20} \text{ cm}^{-3}$  which is close to Fermi stabilization energy ( $E_{FS}$ ) level of CdO, with the assistance of native defects. An amphoteric defects model is used to explain the changing trends in electron concentrations. The tendencies in mobility further confirm our results. This work may provide some strategies to predict the electrical properties in CdO.

**Keywords:** rapid thermal annealing; Hall Effect properties; Fermi stabilization energy; amphoteric defects model



**Citation:** Li, Y.; Chen, G.; Yu, K.; Walukiewicz, W.; Gong, W. Annealing Induced Saturation in Electron Concentration for V-Doped CdO. *Crystals* **2021**, *11*, 1079. <https://doi.org/10.3390/cryst11091079>

Academic Editors: Markus Suta, Nathalie Kunkel and Dechao Yu

Received: 8 June 2021

Accepted: 30 August 2021

Published: 6 September 2021

**Publisher's Note:** MDPI stays neutral with regard to jurisdictional claims in published maps and institutional affiliations.



**Copyright:** © 2021 by the authors. Licensee MDPI, Basel, Switzerland. This article is an open access article distributed under the terms and conditions of the Creative Commons Attribution (CC BY) license (<https://creativecommons.org/licenses/by/4.0/>).

## 1. Introduction

Transparent conductive oxides (TCOs), an attractive type of semiconducting materials that are both optically transparent and electrically conductive, have potential application in optoelectronic devices such as solar cells, photovoltaic, flat panel displays and transparent electrodes [1,2]. Among these TCO materials, Cadmium oxide (CdO) is an n-type II–VI semiconductor with a direct band gap ( $E_g \sim 2.2 \text{ eV}$ ); thus it shows high transparency in the Vis-region. Meanwhile, CdO can achieve even higher conductivity due to its much higher electron mobility with electron concentration [3,4].

It is well known that the electrical properties of CdO film can be tuned through doping with various species and adjusting deposition condition. Intentionally doped CdO with shallow donors (Ga, In and Sn) can get the electron concentration exceeding  $10^{21} / \text{cm}^3$  and electron mobility larger than  $100 \text{ cm}^2 / \text{V-s}$  [5–7]. Vanadium (V) belongs to the 3d transition metal group with  $3d^3 4s^2$  valence electron shell, and V doping introduces highly localized d-levels in V, which probably interact with the original band structure of CdO host [8]. This may lead to different electrical properties. Among various technologies for CdO film preparation, the radio frequency (RF) magnetron sputtering method is widely adapted in industry and considered as a low cost, scalable method [3,9]. The electrical properties of CdO film have been found to be strongly dependent on the RF power, deposition time and deposition atmosphere [10–12].

However, the as-deposited CdO film usually contain many lattice defects, surface defects and internal stress, which will keep the film at an unstable status [9,13]. Thus, improving the stability of CdO film through post-heat treatment is worth investigating. Rapid thermal annealing (RTA) has proved a versatile technique for the post-treatment of semiconductor materials compared to other techniques due to its precise control over the

thermal resources, as well as the annealing atmosphere [13]. To our knowledge, there are few studies about the effect of RTA on V-doped CdO film.

In previous research, we have already studied V doped CdO under ambient Ar deposition [8]. Based on that, Ar/O<sub>2</sub>-deposited Cd<sub>1-y</sub>V<sub>y</sub>O are synthesized as a comparison in this paper. Furthermore, the effects of RTA on the electrical properties of these two series are explored in detail. This work may present further evidence of the position of  $E_{FS}$  in CdO and predict its electrical properties.

## 2. Experimental

V-doped CdO films were deposited on Si glass substrates by rf magnetron sputtering system using CdO target (99.9%) and V<sub>2</sub>O<sub>3</sub> target (99.9%). The chamber was pumped down to 10<sup>-6</sup> Torr before introducing pure Ar (Cd<sub>1-x</sub>V<sub>x</sub>O) and 80%Ar + 20%O<sub>2</sub> (Cd<sub>1-y</sub>V<sub>y</sub>O) sputtering gases. The composition was controlled by varying the sputtering power and target to substrate distance of the individual target. The deposition temperature, time and work pressure were 270 °C, 20 min and 5 mTorr, respectively. The as-grown samples were then rapid-thermally annealed in N<sub>2</sub> ambient. The isochronal annealing was carried out for 20 s at the temperature range of 300~600 °C and isothermal annealing was carried out at ~500 °C for 600 s.

The crystalline phase of as-grown and annealed films was determined by X-ray diffraction (XRD) using a Siemens D500 diffractometer. The film composition and thickness were characterized by Rutherford backscattering spectrometry (RBS) with 3.04 MeV He<sup>++</sup> ion beam. The electrical properties of as-grown and annealed samples were characterized by Hall Effect in Van der Paaw configuration using an Ecopia HMS-3000 system with a 0.6 T magnetic field.

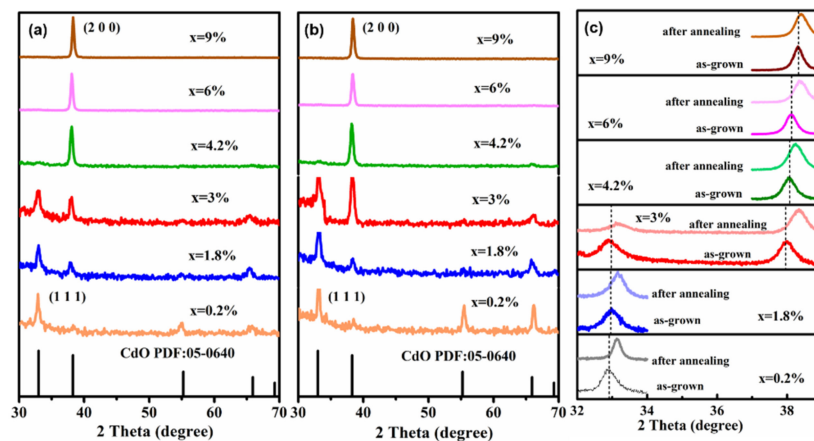
## 3. Results and Discussion

From RBS results, we arrive at the film thickness in the range of 150~200 nm. Meanwhile, the Ar-deposited composition with  $x = 0.2\sim 9\%$  and the Ar/O<sub>2</sub> deposited composition with  $y = 1\sim 4\%$  are also determined.

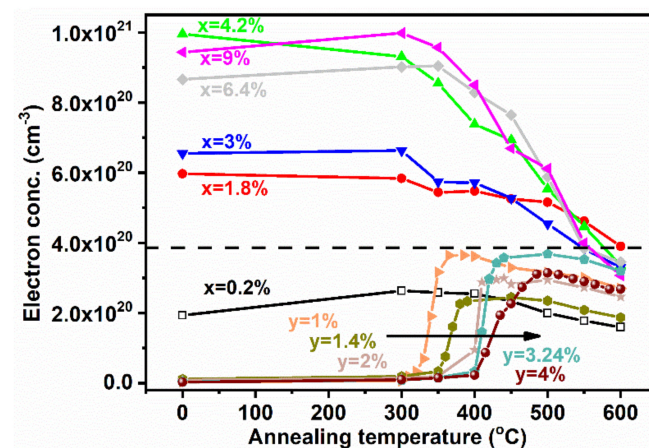
Figure 1a,b show the XRD patterns of as-grown and annealed Cd<sub>1-x</sub>V<sub>x</sub>O ( $x = 0.2\sim 9\%$ ). With increasing V fraction up to 9%, all of the as-grown and annealed films are pure phase and match well with the rocksalt CdO. The preferred orientation in film growth changes gradually from (111) to (200) with increasing V, and the turning point in both of the two series is  $x = 3\%$ . V enter into the CdO lattice and are supposed to substitute for Cd sites based on electronegativity. Comparing the annealed sample with the as-grown one, both of the diffraction peaks (111) and (200) shift to a higher  $2\theta$  angle, as shown in Figure 1c. This can be understood by the Bragg equation:  $2d\sin\theta = n\lambda$ , where  $d$  is the spacing between the planes in the atomic lattice,  $\theta$  is the angle between the incident ray and the scattering planes,  $n$  is an integer, and  $\lambda$  denotes the wavelength of incident wave. Since the ionic radius of V (0.79 Å, 6-coord.) is smaller than Cd (0.95 Å, 6-coord.),  $d$  should decrease with more V substituting for Cd sites, which results in the increase of  $2\theta$ . This indicates that annealing induces mores V substituting for Cd sites. The XRD of Cd<sub>1-y</sub>V<sub>y</sub>O films shows a similar tendency.

Figure 2 shows the effect of annealing temperature on electron concentration in Cd<sub>1-x</sub>V<sub>x</sub>O and Cd<sub>1-y</sub>V<sub>y</sub>O series. As can be seen, all of the initial electron concentrations of Cd<sub>1-x</sub>V<sub>x</sub>O are much higher than that of Cd<sub>1-y</sub>V<sub>y</sub>O. V was supposed to behave as donor for CdO in our previous report, which could donate electrons to the charge carrier. However, a part of V donors is probably passivated by the additional O<sub>2</sub> atmosphere [14,15], thereby lower electron concentration is obtained in Ar/O<sub>2</sub>-deposited samples. The initial electron concentration of 0.2%V-doped CdO (Ar) is as low as the undoped CdO due to the very low doping level, which makes this sample exhibit similar properties as pure CdO with annealing. With increasing annealing temperature, the electron concentrations of Cd<sub>1-x</sub>V<sub>x</sub>O samples with initial values higher than  $4 \times 10^{20} \text{ cm}^{-3}$  show gradual reduction until  $\sim 4 \times 10^{20} \text{ cm}^{-3}$  at 500 °C. Meanwhile, it is noted that Cd<sub>1-y</sub>V<sub>y</sub>O samples exhibit

dramatic increase in electron concentrations until  $\sim 4 \times 10^{20} \text{ cm}^{-3}$  in the temperature range 350–450 °C and then plateau, further increasing temperature results in slightly reduced electron concentrations. Furthermore, it is obvious that the “jump temperature” which is used to describe the rapid increase in electron concentration happening to  $\text{Cd}_{1-y}\text{V}_y\text{O}$  samples gradually increases from 350 °C to 375 °C, 410 °C, 420 °C and 450 °C when increasing the V fraction from 1% to 1.4%, 2%, 3.24% and 4%, respectively. This tendency is represented by the arrow in Figure 2. In summary, after annealing, the high (low) electron concentrations in Ar ( $\text{Ar}/\text{O}_2$ )-deposited V-doped CdO downward (upward) shift to a saturation value at an annealing temperature of 500 °C. In addition, the very low V-doped sample ( $x = 0.2\%$ ) keeps a stable electron concentration at around  $2 \times 10^{20} \text{ cm}^{-3}$  with annealing.



**Figure 1.** XRD of  $\text{Cd}_{1-x}\text{V}_x\text{O}$  ( $x = 0.2\sim 9\%$ ): as-grown films (a); annealed films (b); comparison of as-grown and annealed films in  $2\theta$  range of  $32\sim 39^\circ$  (c).



**Figure 2.** Electron concentrations of  $\text{Cd}_{1-x}\text{V}_x\text{O}$  ( $x = 0.2\sim 9\%$ ) and  $\text{Cd}_{1-y}\text{V}_y\text{O}$  ( $y = 1\sim 4\%$ ) series as a function of annealing temperature when annealed for 20 s.

In order to obtain more detailed information about the saturated electron concentration in these two series, long-time annealing at 500 °C is performed. The saturated electron concentrations, obtained at as long as time as 600 s annealing as a function of V fraction, are shown in Figure 3. Except for the very low V doped sample ( $x = 0.2\%$ ), other Ar-deposited samples with electron concentrations higher than  $4 \times 10^{20} \text{ cm}^{-3}$  and  $\text{Ar}/\text{O}_2$ -deposited samples with electron concentrations lower than  $4 \times 10^{20} \text{ cm}^{-3}$  follow the decreasing and increasing tendencies, respectively. Finally, they saturate at  $\sim 4 \times 10^{20} \text{ cm}^{-3}$ , which can be understood through the amphoteric defect model.

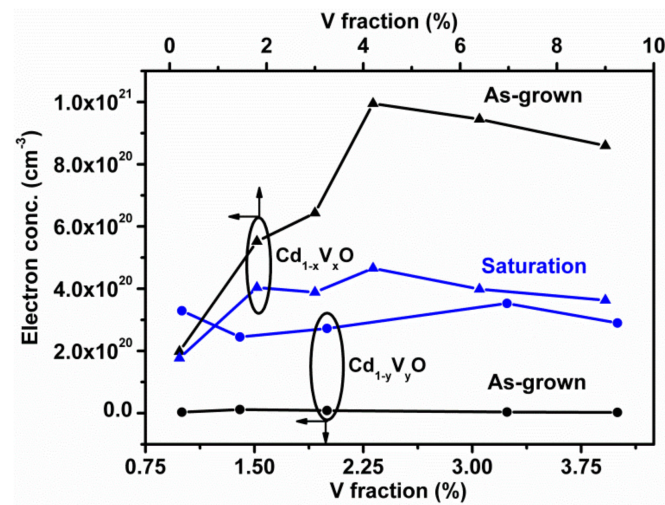


**Figure 3.** Saturated electron concentrations in  $\text{Cd}_{1-x}\text{V}_x\text{O}$  ( $x = 0.2\sim 9\%$ ) and  $\text{Cd}_{1-y}\text{V}_y\text{O}$  ( $y = 1\sim 4\%$ ) series; as-grown are also shown.

Figure 4 gives the simplified amphoteric defect model of CdO [16,17]. The formation energy for donor (acceptor) native defects increases (decreases) with the increasing Fermi level, such that formation of donor (acceptor) native defects is most favorable when the Fermi level is below (above) an energy level known as the Fermi-level stabilization energy ( $E_{FS}$ ) [16,17], denoted as the white dashed line in Figure 4. This level makes the energy at which their character changes, from predominantly donor-like (valence band character) below  $E_{FS}$  to predominantly acceptor-like (conduction band character) above the  $E_{FS}$  [17]. Consequently, we can obtain the equal formation energies for donor and acceptor native defects at  $E_{FS}$ , which means the number of formed donors can balance with that of formed acceptors and no change happens in carrier density when further creating native defects at this point [17]. The  $E_{FS}$  is located substantially above the conduction band minimum (CBM) in CdO due to its extremely low CBM, which is different to most conventional semiconductors whose  $E_{FS}$  is normally located close to the middle of the fundamental band gap [18]. This particular location of  $E_{FS}$  in CdO results in the formation energy for compensating acceptor (donor) defects being relatively high (low) with n-type (p-type) doping, allowing CdO to be extrinsically heavily n-type doped, thus p-type CdO is always difficult to achieve [19]. The exact location of  $E_{FS}$  in CdO has been determined through the ionic irradiation induced defects which results in the electron concentration stabilizing at a saturation level of  $\sim 5 \times 10^{20} \text{ cm}^{-3}$  [20]. Our annealed results are close to  $E_{FS}$  of CdO. RTA can fulfill high temperature annealing in a very short time, which results in the reduced defects and improved crystallization properties with minimal dopant redistribution [21]. The thermal energy provided by RTA is able to induce the thermodynamic system to reach equilibrium. Combined with the amphoteric defect model, the electron concentrations of Ar-deposited  $\text{Cd}_{1-x}\text{V}_x\text{O}$  ( $x > 0.2\%$ ) series with value higher than  $4 \times 10^{20} \text{ cm}^{-3}$  have the tendency to go down and saturate at  $E_{FS}$  level with the assistance of native acceptors (V vacancy, Cd vacancy or O interstitial) after annealing. As a result, the electron concentrations of these samples stabilize near  $E_{FS}$  after long-time annealing at  $500^\circ\text{C}$ . However, the electron concentrations of  $\text{Cd}_{1-y}\text{V}_y\text{O}$  series with low original electron concentrations in the range of  $10^{18}\sim 10^{19} \text{ cm}^{-3}$  show rapid increase at certain points and then saturate close to the  $E_{FS}$  level with time-dependent annealing. During the annealing process, some passivated V species are probably activated under  $\text{N}_2$  background, then behave as donors to donate electrons to the charge carrier, resulting in increased electron concentrations.

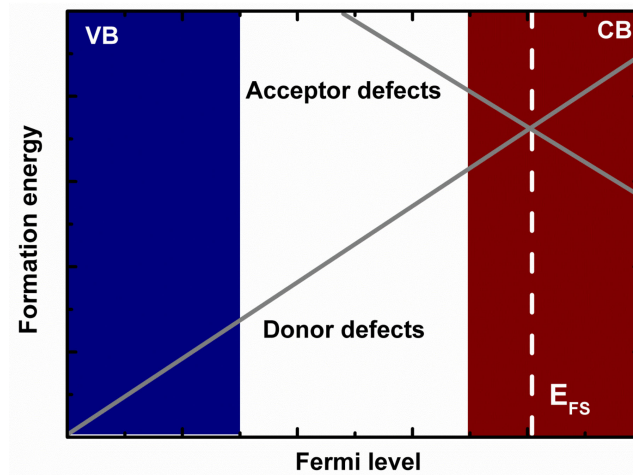


**Figure 4.** Schematic representation of the formation energy as a function of Fermi level in CdO. The CB and VB are represented by red and blue shading, respectively.

It is worth noting that the “jump temperature” increases from 350 °C to 450 °C with increasing V concentration in  $\text{Cd}_{1-y}\text{V}_y\text{O}$  series. This means the barrier energy enhances gradually with V doping, which can be calculated through the Arrhenius equation [22].

$$1 = w_{OPF} \times \exp\left(\frac{-\Delta E}{k_B T}\right) \quad (1)$$

where  $w_{OPF}$  is the optical phonon frequency of CdO with a value of  $9.06 \times 10^{13} \text{ s}^{-1}$ ,  $k_B$  is Boltzmann constant,  $T$  is the temperature to overcome the energy barrier and  $\Delta E$  is the barrier energy. As a result, the calculated  $\Delta E$  increases linearly from 1.72 eV to 1.79 eV, 1.89 eV, 1.91 eV and 2.00 eV with the V fraction increasing from 1% to 1.4%, 2%, 3.24% and 4%, respectively, indicating that more energy is required to overcome the barrier in order to reach equilibrium when increasing doped V. The reason for the very low V-doped sample ( $x = 0.2\%$ ), almost keeping stable electron concentration at around  $2 \times 10^{20} \text{ cm}^{-3}$  with annealing, is because the doped V level is too low to influence the basic electrical properties of CdO.

Based on the above discussion, it is reasonable to check the mobility tendencies to confirm our deduction. Figure 5a,b show the saturated mobility of  $\text{Cd}_{1-x}\text{V}_x\text{O}$  and  $\text{Cd}_{1-y}\text{V}_y\text{O}$  after long time annealing at 500 °C, respectively. As-grown mobility is also shown as references. For  $\text{Cd}_{1-x}\text{V}_x\text{O}$ , the mobility exhibits fast reduction after annealing and becomes smaller than the as-grown ones when  $x > 0.2\%$ , even though RTA could increase the mobility through reduced defects and improved crystallization properties, which is confirmed by the enhanced mobility in the  $x = 0.2\%$  sample after annealing. However, for Ar/ $\text{O}_2$ -deposited series, mobility increases greatly after annealing. From the amphoteric defect model, it has been suggested that the nature of formed native defects in Ar-deposited series is acceptor and in Ar/ $\text{O}_2$ -deposited series is donor. Both electron concentration and scattering centers are strongly dependent on the formed defects, which can be expressed as [23].

$$n = d - a \quad (2)$$

$$N_i = d + a \quad (3)$$

where  $d$  and  $a$  denote the number of donors and acceptors, respectively,  $n$  is electron concentration and  $N_i$  is scattering centers. As the favorably formed defects, acceptors in Ar-deposited series increase greatly after annealing, meanwhile reducing the electron concentration, which is in accord with the result in Figure 2. On the other hand, the increased acceptors would produce more scattering centers and then reduce mobility. Such an effect surpasses the improved mobility from better crystalline, and overall exhibits rapid

reduction in mobility. This tendency further confirms the conclusion from the amphoteric defect model. For Ar/O<sub>2</sub>-deposited samples, donors are the usually formed defects after annealing. From Equation (3), the increased donors are expected to increase scattering centers and then reduce mobility if no change happens to the acceptors. However, the mobility increases greatly after annealing; this indicates that more acceptors may disappear in this process, which could compensate partly for the donors. As a result, the overall scattering centers decrease and mobility increases. On the other hand, the combined effects of increased donors and reduced acceptors could finally result in the enhanced electron concentration from Equation (2). This is also verified in Figure 2.

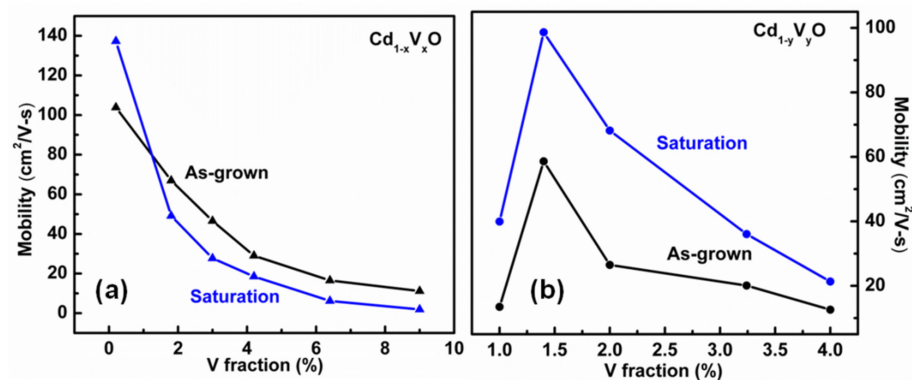


**Figure 5.** As-grown and saturated mobility in Cd<sub>1-x</sub>V<sub>x</sub>O ( $x = 0.2\sim 9\%$ ) (a) and Cd<sub>1-y</sub>V<sub>y</sub>O ( $y = 1\sim 4\%$ ) series (b).

#### 4. Conclusions

Ar-deposited Cd<sub>1-x</sub>V<sub>x</sub>O and Ar/O<sub>2</sub> deposited Cd<sub>1-y</sub>V<sub>y</sub>O show higher and lower electron concentrations than  $4 \times 10^{20} \text{ cm}^{-3}$ , respectively. V behave as donors for CdO which are probably passivated by O<sub>2</sub> in the synthesis process, resulting in much lower electron concentrations in Ar/O<sub>2</sub>-deposited series than in Ar-deposited series. After annealing in N<sub>2</sub>, the electron concentrations of the two series reduce or increase to a saturated value of  $\sim 4 \times 10^{20} \text{ cm}^{-3}$ , which is close to  $E_{FS}$ . Based on the amphoteric defect model, the favorably formed defects for Ar-deposited and Ar/O<sub>2</sub>-deposited series during annealing are acceptors and donors, respectively. This is also confirmed through the combined results of the changing tendency in electron concentration and mobility.

**Author Contributions:** Conceptualization: Y.L.; Data curation: G.C.; Formal analysis: K.Y.; Resources: W.W.; Software: W.G. All authors have read and agreed to the published version of the manuscript.

**Funding:** This research was funded by National Natural Science Foundation of China (No. 51602121) and PhD Start-up Program of Huizhou University (No. 2016JB006).

**Institutional Review Board Statement:** Not applicable.

**Informed Consent Statement:** Not applicable.

**Data Availability Statement:** The data presented in this study is available within the article.

**Acknowledgments:** This work was supported by the U.S. Department of Energy, Office of Science, Basic Energy Sciences, Materials Sciences Engineering Division, China Scholarship Council, National Natural Science Foundation of China (No. 51602121), Guangdong Provincial Natural Science Foundation Project (No.2021A1515010282) and PhD Start-up Program of Huizhou University (No. 2016JB006). This work was also supported by Program for Innovative Research Team of Guangdong Province & Huizhou University (IRTHZU).

**Conflicts of Interest:** The authors declare no conflict of interest.

## References

1. Ismail, R.A. Improved characteristics of sprayed CdO films by rapid thermal annealing. *J. Mater. Sci. Mater. Electron.* **2019**, *20*, 1219–1224. [[CrossRef](#)]
2. Franco-Linton, B.; Castanedo-Pérez, R.; Torres-Delgado, G.; Márquez-Marín, J.; Zelaya-Ángel, O. Influence of vacuum and Ar/CdS atmospheres-rapid thermal annealing (RTA) on the properties of Cd<sub>2</sub>SnO<sub>4</sub> thin films obtained by sol-gel technique. *Mater. Sci. Semicond. Process.* **2016**, *56*, 302. [[CrossRef](#)]
3. Xie, M.T.; Zhu, W.; Yu, K.M.; Zhu, Z.S.; Wang, G.Z. Fe-embedded Au (111) monolayer as an electrocatalyst for N<sub>2</sub> reduction reaction: A first-principles investigation. *J. Alloys Compd.* **2019**, *776*, 259. [[CrossRef](#)]
4. Morales, G.E.M.; Garcia, M.E.A.; Cruz, S.C.; Plata, B.R.; Moreno, O.P.; Pérez, R.G. CdCO<sub>3</sub> nanocrystalline thin film grown by chemical bath and its transition to porous CdO by thermal annealing treatment. *Optik* **2018**, *171*, 347–355. [[CrossRef](#)]
5. Yu, K.M.; Detert, D.M.; Chen, G.B.; Zhu, W.; Liu, C.P.; Grankowska, S.; Hsu, L.; Dubon, O.D.; Walukiewicz, W. Defects and properties of cadmium oxide based transparent conductors. *J. Appl. Phys.* **2016**, *119*, 18150. [[CrossRef](#)]
6. Yu, K.M.; Mayer, M.A.; Speaks, D.T.; He, H.; Zhao, R.; Hsu, L.; Mao, S.S.; Haller, E.E.; Walukiewicz, W. Ideal transparent conductors for full spectrum photovoltaics. *J. Appl. Phys.* **2012**, *111*, 123505. [[CrossRef](#)]
7. Segura, A.; Sanchez-Royo, J.F.; Garia-Domene, B.; Almonacid, G. Current underestimation of the optical gap and Burstein-Moss shift in CdO thin films: A consequence of extended misuse of  $\alpha^2$ -versus-hv plots. *Appl. Phys. Lett.* **2011**, *99*, 151907. [[CrossRef](#)]
8. Li, Y.J.; Yu, K.M.; Chen, G.B.; Liu, C.P.; Walukiewicz, W. Conduction band modifications by d states in vanadium doped CdO. *J. Alloys Compd.* **2020**, *822*, 153567. [[CrossRef](#)]
9. Yu, J.H.; Kim, J.H.; Park, D.S.; Jeong, T.S.; Youn, C.J.; Hong, K.J. Effect of rapid thermal annealing on Zn<sub>1-x</sub>Cd<sub>x</sub>O layers grown by radio-frequency magnetron co-sputtering. *Cryst. Res. Technol.* **2010**, *45*, 1050–1056. [[CrossRef](#)]
10. Sakthivel, P.; Murugan, R.; Asaithambi, S.; Karuppaiah, M.; Rajendran, S.; Ravi, G. Radio frequency magnetron sputtered CdO thin films for optoelectronic applications. *J. Phys. Chem. Solids* **2019**, *126*, 1–10. [[CrossRef](#)]
11. Saha, B.; Thapa, R.; Chattopadhyay, K.K. Wide range tuning of electrical conductivity of RF sputtered CdO thin films through oxygen partial pressure variation. *Sol. Energy Mater. Sol. Cells* **2008**, *92*, 1077–1080. [[CrossRef](#)]
12. Sakthivela, P.; Murugana, R.; Asaithambiah, S.; Karuppaiah, M.; Rajendrana, S.; Ravi, G. Influence of radiofrequency power on structural, morphological, optical and electrical properties of magnetron sputtered CdO: Sm thin films as alternative TCO for optoelectronic applications. *J. Alloys Compd.* **2018**, *765*, 146. [[CrossRef](#)]
13. Devika, M.; Koteeswara, N.; Reddy, S.; Venkatramana Reddy, K.; Ramesh, K.; Gunasekhar, R. Influence of rapid thermal annealing (RTA) on the structural and electrical properties of SnS films. *J. Mater. Sci. Mater. Electron.* **2009**, *20*, 1129. [[CrossRef](#)]
14. Huang, T.Z.; Yuan, X.X.; Yu, J.M.; Wu, Z.; Han, J.T.; Sun, G.X.; Xu, N.X.; Zhang, Y.H. Effects of annealing treatment and partial substitution of Cu for Co on phase composition and hydrogen storage performance of La<sub>0.7</sub>Mg<sub>0.3</sub>Ni<sub>3.2</sub>Co<sub>0.35</sub> alloy. *Int. J. Hydrogen Energy* **2012**, *37*, 1074. [[CrossRef](#)]
15. Silversmit, G.; Depla, D.; Poelman, H.; Marin, G.B.; Gryse, R.D. Determination of the V2p XPS binding energies for different vanadium oxidation states (V<sup>5+</sup> to V<sup>0+</sup>). *J. Electron Spectrosc. Relat. Phenom.* **2004**, *135*, 167–175. [[CrossRef](#)]
16. Kwon, H.; Thompson, L.T.; Eng, J., Jr.; Chenz, J.G. n-Butane dehydrogenation over vanadium carbides: Correlating catalytic and electronic properties. *J. Catal.* **2000**, *190*, 60–68. [[CrossRef](#)]
17. Walukiewicz, W. Amphoteric native defects in semiconductors. *Appl. Phys. Lett.* **1989**, *54*, 2094–2096. [[CrossRef](#)]
18. King, P.D.C.; Veal, T.D.; Jefferson, P.H.; Zúñiga-Pérez, J.; Muñoz-Sanjosé, V.; McConville, C.F. Unification of the electrical behavior of defects, impurities, and surface states in semiconductors: Virtual gap states in CdO. *Phys. Rev. B* **2009**, *79*, 035203. [[CrossRef](#)]
19. Langer, J.M.; Delerue, C.; Lannoo, M. Transition-metal impurities in semiconductors and heterojunction band lineups. *Phys. Rev. B* **1998**, *38*, 7723. [[CrossRef](#)] [[PubMed](#)]
20. Burbano, M.; Scanlon, D.O.; Watson, G.W. Sources of conductivity and doping limits in CdO from hybrid density functional theory. *J. Am. Chem. Soc.* **2011**, *133*, 15065–15072. [[CrossRef](#)]
21. Speaks, D.T.; Mayer, M.A.; Yu, K.M.; Mao, S.S.; Haller, E.E.; Walukiewicz, W. Fermi level stabilization energy in cadmium oxide. *J. Appl. Phys.* **2010**, *107*, 113706. [[CrossRef](#)]
22. Seidel, T.E.; Lischner, D.J.; Pai, C.S.; Lau, S.S. Temperature transients in heavily doped and undoped silicon using rapid thermal annealing. *J. Appl. Phys.* **1985**, *57*, 1317–1321. [[CrossRef](#)]
23. Laidler, K.J. The development of the Arrhenius equation. *J. Chem. Educ.* **1984**, *61*, 494. [[CrossRef](#)]